PERGAMON

International Journal of Heat and Mass Transfer 45 (2002) 2031–2042

International Journal of HEAT and MASS TRANSFER

www.elsevier.com/locate/ijhmt

Forced convection heat transfer at an inclined and yawed round tube

Mao-Yu Wen *, Kuen-Jang Jang

Department of Mechanical Engineering, Cheng-Shiu Institute of Technology, Kaohsiung 833, Taiwan, ROC

Received 30 December 2000; received in revised form 28 September 2001

Abstract

Experiments have been performed to determine the heat transfer coefficients for forced convection airflow over a cylindrical obstacle that is inclined and yawed relative to the oncoming flow. The experiments encompassed a wide range of angles of attack and angles of yaw, and extended over a Reynolds number ranging from about 1000 to 7000. It was found that owing to three-dimensional flow effects, the heat transfer coefficients were remarkably insensitive to both the angle of attack and the angle of yaw. This enabled all the results to be correlated by the equation $\overline{Nu(Z)} = 0.182Re^{0.63}Pr^{1/3}$ with an accuracy of $\pm 4\%$. This investigation also introduces a factor ($C_\theta = \overline{Nu(Z)}/\overline{Nu(Z)}_{\theta=90^\circ}$) which can be used for finding the heat transfer on a tube positioned at different angles to the flow direction. No perceptible dependence of C_θ on Re was detected. In addition, flow visualizations were explored to broaden our fundamental understanding of the heat transfer outside the tube.

1. Introduction

Ribs/fins are widely used to increase the rate of heat transfer from a wall surface. In many industrial applications such as electronic components, automobile radiators, aerospace, air-conditioning, and heat exchangers in vessels, the weight of the available space is a primary design consideration. As the increase in heat transfer rate is accompanied by a friction factor increase [1], the preferred roughness geometry will yield the desired heat transfer augmentation with a minimum friction factor. The internal passages can be approximately modeled as square or rectangular channels with two opposite rib-roughened walls/fins. The heat transfer and friction characteristics in these channels are different from those of circular tubes, parallel plates, or annuli.

In the fundamentals of heat transfer characteristics of fins, Kern and Kraus [2] gave a thorough treatment for the optimum design of convecting fins. A comprehensive review of fin technology was presented by Kraus [3] for over six decades. In forced convection, Dhar and Arora [4] obtained the optimum fin profile and concluded that the use of individually optimum-profile fins did not necessarily result in the optimum finned surfaces. The least material of convectively cooled arrays of longitudinal, rectangular fins was theoretically proposed by Bar-Cohen and Jelinek [11]. Gee and Webb [6] conducted experimental works to study the effect of rib helix angle on turbulent heat transfer and friction for fully developed flows in circular tubes. One rib pitch-to-height ratio ($p/e = 15$) and three rib helix angles (30°, 49°, and 70°) were examined. The results showed that the helical rib-roughness, and the preferred helix angle was approximately 49°. Han and Park [7] further investigated the combined effects of the rib angle of attack ($\theta = 30°$, 45°, 60°, and 90°) and the channel aspect ratio (AR = 1, 2, and 4) on the local heat transfer coefficient in rectangular channels with two opposite ribbed walls for developing and fully developed turbulent flows under sudden entrance condition. In their study, it was found that the best heat transfer performance in the square channel with angled ribs ($\theta = 30$–35°) was about 30% higher than that with the transverse ribs (90°) for a constant pumping power. However, in the rectangular ducts (AR = 2 and 4) at 30–45° it was only 5% higher than that at $\theta = 90°$.

* Corresponding author. Tel.: +886-7-733-7100; fax: +886-7-733-7100.

E-mail address: wmy@cc.csit.edu.tw (M.-Y. Wen).

0017-9310/02/$ - see front matter
PII: S0017-9310(01)00308-8

Nomenclature

A	surface area of a heated tube [m^2]
C_p	specific heat [J kg^{-1} °C]
C_θ	ratio of the heat transfer from a tube at arbitrary θ to that from a tube at $\theta = 90°$
D	tube outer diameter [m]
D_h	duct hydraulic diameter without elements [m]
h	convection heat transfer coefficient [W m^{-2} °C]
$\bar{h}$	average convection heat transfer coefficient [W m^{-2} °C]
k_f	thermal conduction of the fluid [W m^{-1} K^{-1}]
L	length of the test tube [m]
Nu	Nusselt number $= hD_h/k_f$
$\overline{Nu}$	average Nusselt number $= \bar{h}D_h/k_f$
Pr	Prandtl number $= v/\alpha$
Q	heat flux [W]
Re	Reynolds number $= UD_h/v$
T_{bi}	inlet bulk mean temperature of the fluid [°C]
T_{bo}	outlet bulk mean temperature of the fluid [°C]
T_f	reference fluid temperature, $0.5(T_{wz} + T_{bz})$ [°C]
T_{wz}	average circumference-wall temperature at any Z [°C]
U	inlet velocity of the air in the test tube [m s^{-1}]
X	streamwise direction coordinate [m]
Y	transverse coordinate [m]
Z	axial coordinate ($Z = 0$ at heated test section inlet reference) normal to the bottom of the test channel [m]

Greek symbols

μ	viscosity [kg m^{-1} s^{-1}]
v	kinematic viscosity [m^2 s^{-1}]
α	thermal diffusivity [m^2 s^{-1}]
ϕ	angle of yaw
θ	angle of attack
ρ	density [kg m^{-3}]

Subscripts

b	bulk mean
i	inlet
m	mean
max	maximum
min	minimum
o	outlet
w	wall

However, all the foregoing methods are essentially applicable for the case of a single tube (fin). Most heat transfer surfaces are made up of round tubes due to the simplicity of their manufacture and installation. The research to be reported here is a study of the heat transfer characteristics of boundary layer flows subjected both to yaw and to an angle of attack. It is well known that the ribs/fins can break up the viscous sublayer of the flow and more and promote local wall turbulence that, in turn, increases the heat transfer from the rib/fin. In addition, a thermally conductive rib/fin attached to the heated wall provides a greater surface area for heat transfer over that of a ribless wall. An elliptic cylinder is a general form, which becomes a flat or a circular cylinder depending on the ratio of the major to minor axes (see Fig. 1). Fig. 1 shows top views of tilted, round tubes – which take the appearance of elliptic tubes. There may be an advantage to using elliptic tubes, since the pumping power needed to flow fluids around them may become very small. There have been a number of studies [8–10] on the characteristics of the flow field and heat transfer adjacent to a bare elliptic tube.

Realizing the potential of air cooling, the present work was aimed at an experimental study of air cooling of a single round tube of heat source mounted on the bottom of a rectangular flow channel, as sketched in Fig. 2. Experimental work on forced convective cooling airflow over a inclined and yawed cylinder is sparse, and little work exists with a single round tube on the bottom of channel to which a heated water chamber was fixed. This study assesses the importance of various geometrical parameters (attack angle θ and yaw angle ϕ) (see Fig. 2) for the present study, since the underlying effects are still not well understood. The conjugate nature of the problem, arising due to coupling between convection in the fluid and conduction in the sources, is considered in the interpretation of the results. Correlating equations are obtained to predict heat transfer rates for different circumstances. Furthermore, flow visualization studies on a single tube mounted on the lower wall have been complemented.

2. Description of experiment

2.1. Experimental apparatus and procedures

A horizontal low-speed wind tunnel was used for the heat transfer, as shown schematically in Fig. 2(a). As can be seen in the diagram, the experimental system consisted of the following main components: test section, main/minor wind tunnels, flow straightener, flow meter blower, and water pumping system. The test section with a 72 mm × 35 mm cross-section was constructed of acrylic, and calibrated static pressure taps were located upstream and downstream of the test section. Cold air

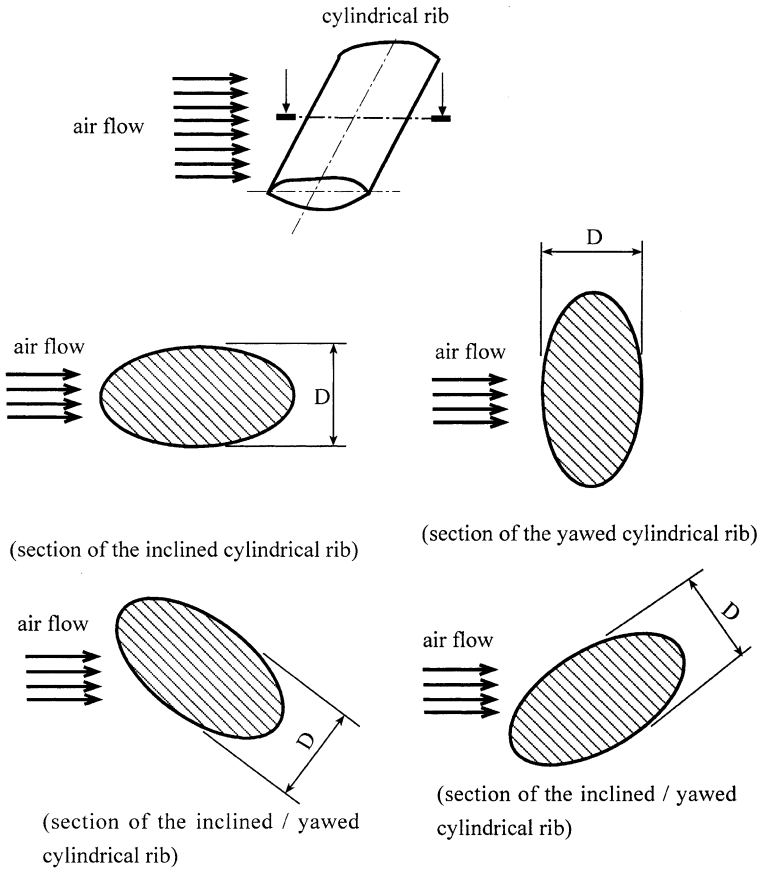

Fig. 1. The various section types of the inclined/yawed cylindrical rib (top views).

flowing through the main wind tunnel was driven by a 0.5 HP frequency adjusted low-speed axial blower, and hot water flowing through the water chamber was driven by a 1 HP pump. The test section was constructed by using a commercial plexiglass plate 10 mm thick. The test section was 35 mm wide, 72 mm high and 870 mm long. In order to provide a constant temperature on the lower surface, a heated water chamber was fixed to the bottom of the lower plate as shown in Fig. 2. The free-stream turbulence level in the test section was less than 0.75%, and the uniformity of the test section exceeded 96%. A model cylinder (12 mm diameter and 133 mm high) was attached normal to the lower plate (see Fig. 2). The free-stream velocity was varied by throttling the inlet of the fan.

The temperature distribution for the present system was measured by a total of 58 alumel–chromel thermocouples of 0.5 mm $\varnothing$ imbedded in the wall, as illustrated in Fig. 3. The thermocouple beads were carefully imbedded into the wall and then ground flat to the surface. The thermocouple lead wires were connected to a recorder (180 mm Hybird recorder, AH3000, Chino) and a precision anemometer (avm-03).

To examine the flow structure, flow visualization experiments were conducted for a single tube mounted on the wall. The smoke coming from a smoke generator and air as the convection medium were used to visualize the flow. The illumination of the smoke was done by using a slide projector as a light source shining through a narrow slit so as to produce a plane of light. All photographs were taken with a Canon AE1 camera on FUJICOLOR ISO 100 film with exposure time of 1/8–1/15 s.

2.2. Uncertainty and data reduction

Different angles of yaw and angles of attack relative to the oncoming flow were tested for a single tube mounted on the wall. The overall heat transfer results were evaluated by averaging the average heat transfer for the main wind tunnel. An uncertainty analysis was also carried out based on the work of Kline and McClintock [5]. Uncertainties in heat transfer coefficient, Nusselt number, and Reynolds number were evaluated.

The experimentally determined average heat transfer coefficients were recast in dimensionless form in terms of the Nusselt number

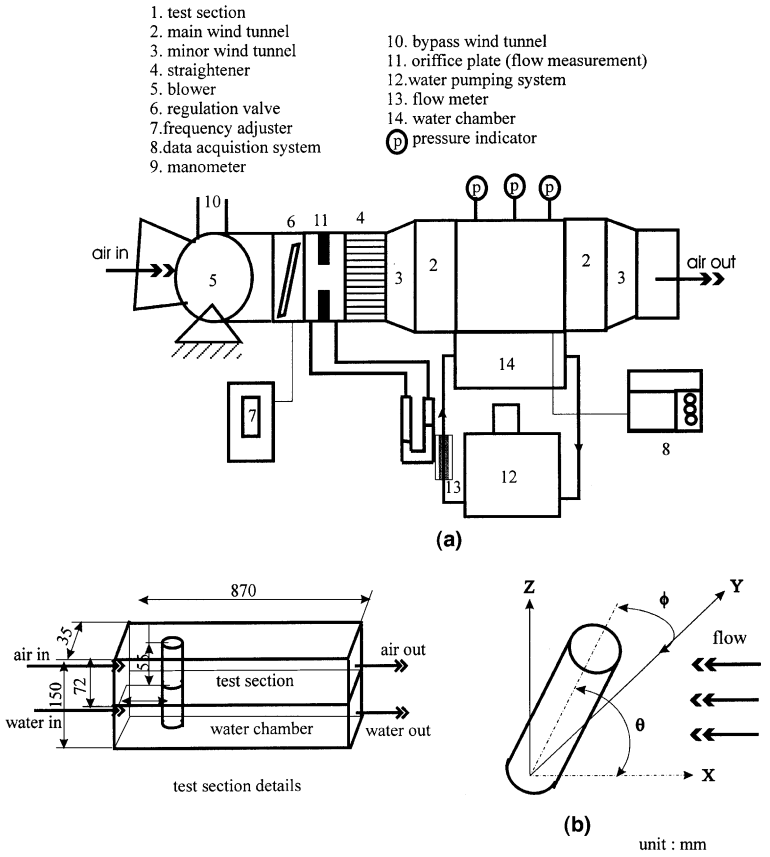

Fig. 2. (a) Schematic view of experimental apparatus. (b) Illustration of the angle of attack (θ) and the angle of yaw (ϕ).

$$\overline{Nu(Z)} = \frac{\bar{h}D_h}{k_f} = \left(\frac{Q}{\pi DL}\right)\left(\frac{1}{L}\int_0^L \frac{dz}{T_{wz}-T_{bz}}\right)\left(\frac{D_h}{k_f}\right), \quad (1)$$

where $Q = \dot{m}C_p(T_{bo} - T_{bi})$. The local values of the thermophysical properties of air were obtained at a reference fluid temperature of $T_f = 0.5(T_{wz} + T_{bz})$. The T_{wz} is an average of four circumferenced wall temperatures at a fixed position of the z direction (shown in Fig. 3). The bulk temperature T_{bz} at a certain z position is roughly evaluated by an average of the local fluid temperatures for the section of the thermocouple position (the thermocouple arrangements for present study were shown in Fig. 3). Uncertainty in the measurement of the temperature difference was ± 0.2 °C for the instrumentation used here. Uncertainty in temperature is the major contributor to the uncertainty in h. The estimated uncertainty in the h results in a maximum value of 2.3%. For the experiments with air, variations among the measured temperatures for a given run were less than $\pm 0.7\%$ of the mean wall-to-bulk temperature difference. D_h is the duct hydraulic diameter without elements. Again, the uncertainties in the module dimensions and the thermal conductivity form a very small part of the total uncertainty in Nu. It remains almost the same as that in heat transfer coefficient. The Reynolds number for flow through the test section is given by

$$Re = \rho U D_h/\mu, \quad (2)$$

where U is the average inlet velocity of the fluid. The Reynolds number is based on the hydraulic diameter D_h. The major uncertainty comes from that in the volumetric flow rate. The uncertainty is about 3% in Re. It is a constant for all the runs.

3. Experimental results and discussion

A series of tests were carried out for forced convection airflow over a cylindrical obstacle inclined and yawed relative to the oncoming flow at various constant airflow velocity conditions. The parameters that were varied during the course of the experiments included the Reynolds number, the angle of attack and the angle of yaw (Fig. 2(b)). The Reynolds number spanned the

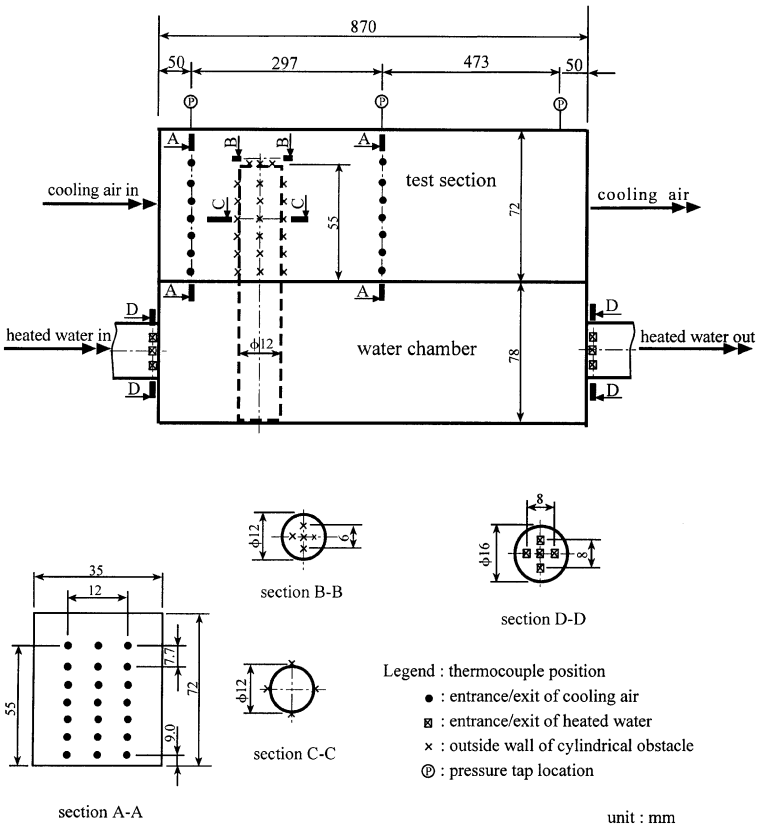

Fig. 3. Details of position for quantitative temperature and pressure measurements.

range between about 1000 and 7000. For the angle of attack, values of 45°, 60°, 75°, 90°, 105°, 120° and 135° were chosen. With regard to yaw, the symmetry of the geometry requires that only angles 45°, 60°, 75°, and 90° be considered. There were 150 different cases to be tested to gather extensive data for analyzing experimental information of the heat transfer. In addition, 14 flow field visualizations were presented and discussed in this study. Examination of flow uniformity for the cold air at inlet by using the pitot tube and hot wire found that the flow uniformity of the cold air at inlet was acceptable. The performance of the apparatus and the measuring technique were deemed satisfactory. The energy gained by the air across the entire test section was compared to the heat gained by the hot water pumping system. For all these tests, the analysis found that the energy balance was satisfied within 6.9%.

3.1. Flow visualization

Figs. 4 and 5 show the photos of streakline patterns of a smoke–air mixture over a cylinder. Such a flow visualization study not only exhibits salient features of the horseshoe vortex around individual rib elements but also reveals qualitative information concerning convective transport. Comparing Figs. 4(a) and (b), as known, at low Re ($Re = 5$) (Fig. 4(a)), a flow over a cylinder produces a smooth pattern and the boundary layer is separated from the surface only near the rear stagnation point of the cylinder. For high Re, inertia forces start playing an increasingly perceptible role as Re rises. In Fig. 4(b) ($Re = 1020$), the laminar boundary layer separates from the surface near the center part of the cylinder and a vortex flow (wake) sets on over the back of the cylinder. As Re is increased further, the boundary layer gradually becomes turbulent and the point of its separation is shifted in the direction of the rear stagnation point (not shown here). As known, the flow over a cylinder at 90° angle of attack (Fig. 4(c)) also produces a smooth pattern and the layer separates from the surface near the center part of the cylinder and a vortex flow (wake) sets on over the back of the cylinder. As the angle of attack is increased further, for Fig. 4(d)–(f) both size and strength (the angular speed of the vortex) in the flow patterns are also increased.

Fig. 5 displays the smoke patterns and schematic representation with different yaw angle at $Re = 1020$ for (a) top view, and (b) front view. Taking a detailed

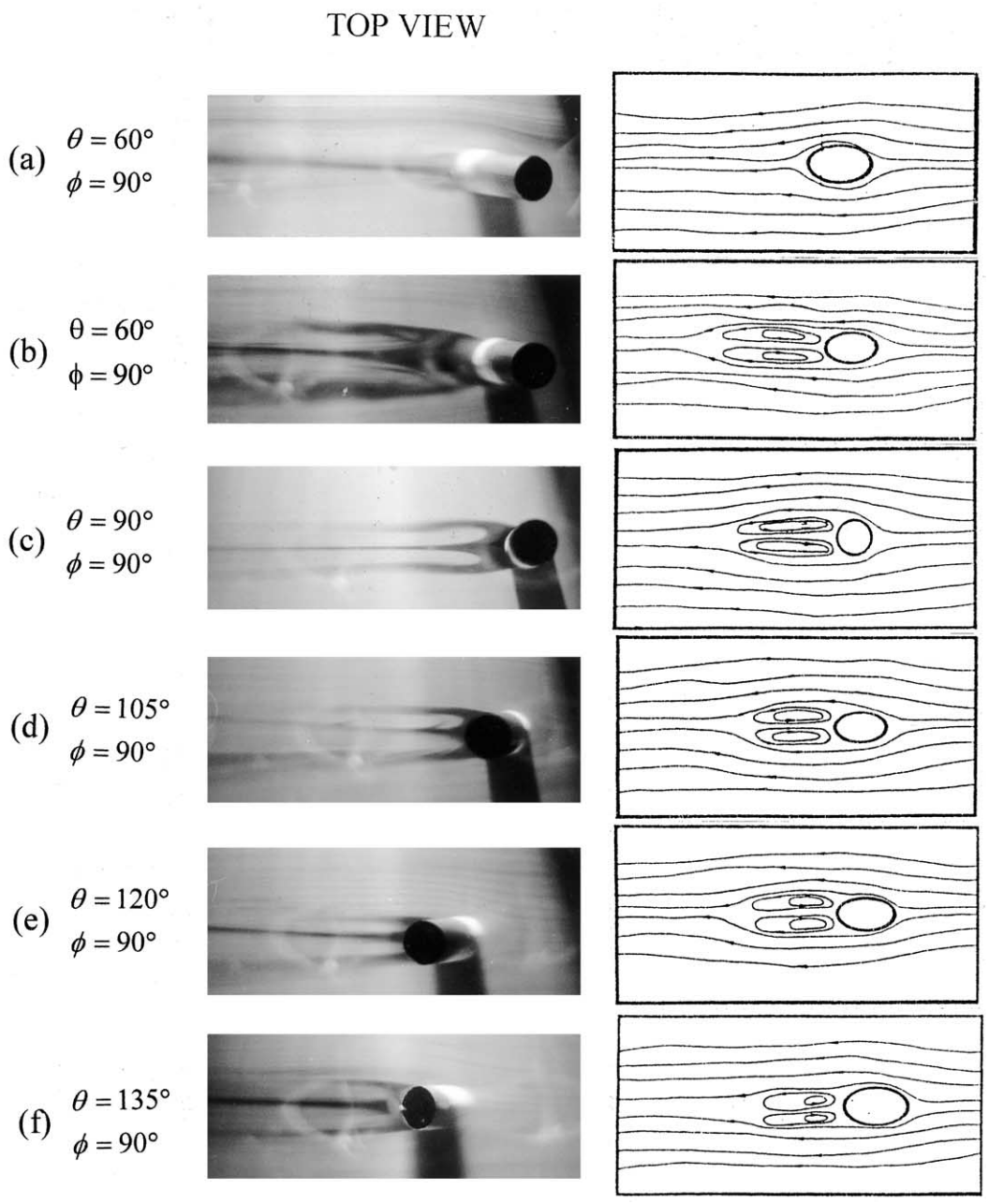

Fig. 4. Smoke patterns and schematic representation with different attack angles at (a) $Re = 5$ and (b)–(f) $Re = 1020$.

examination, Fig. 5(left) shows the horseshoe vortices in the stagnation area and the wake of the tube back increase with decreasing yaw angle ($\phi \leqslant 90°$) at $Re = 1020$. In addition, from Fig. 5(right), it is seen that the strength of the vortex within the restricted region (an angular geometry formed by a horizontal wall subjected to an inclined tube) increases with decreasing yaw angle.

For present airflow over a cylinder obstacle, the cylinder enlarges the heat transfer area and thereby reduces the air-side thermal resistance. The structure of the air flow is complex. It consists of horseshoe vortices in the stagnation area and flow separation in the wake of the tube. The horseshoe vortex introduces additional mixing of the fluid and thus increases strongly the cylinder heat transfer in the stagnation area. The two

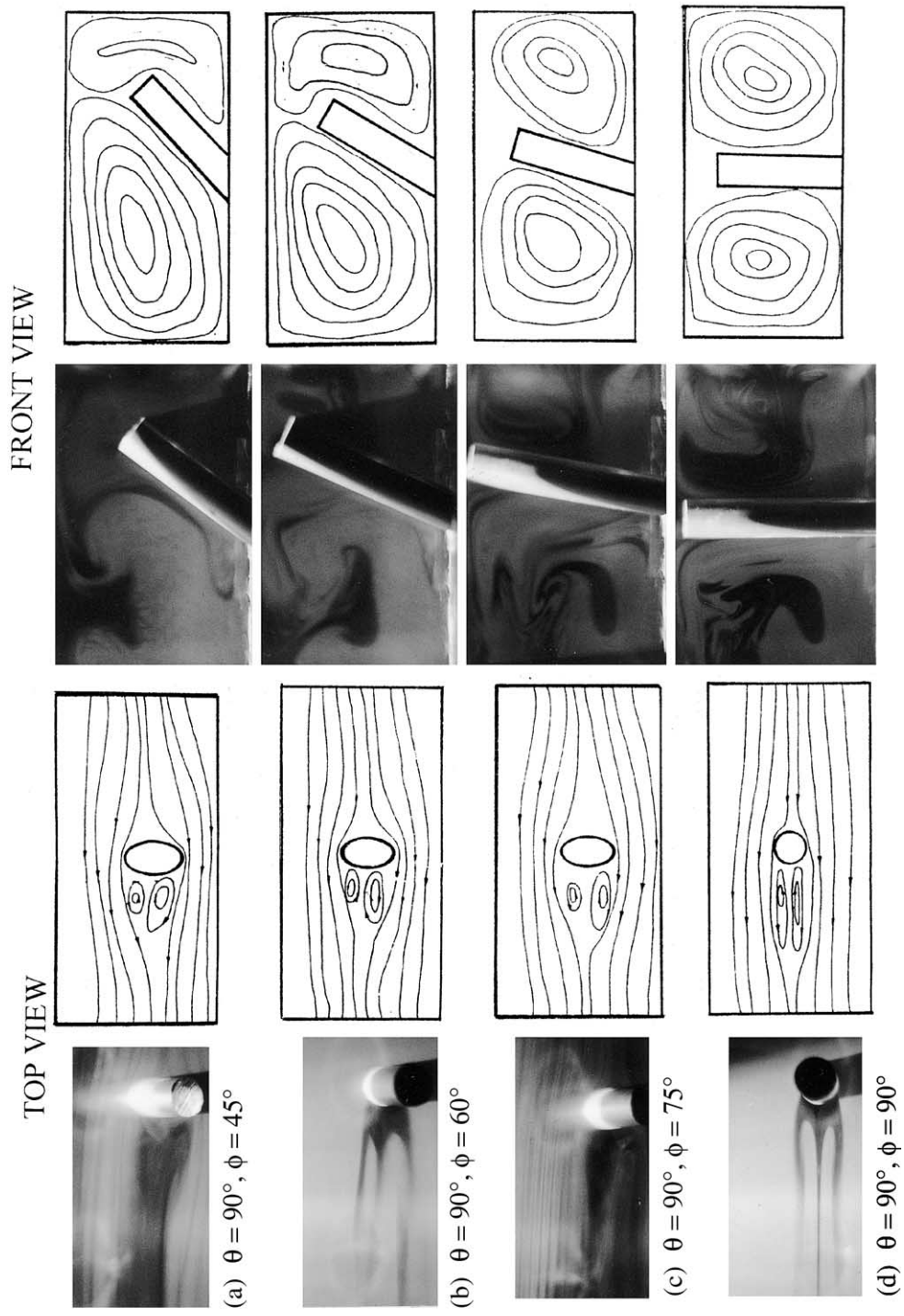

Fig. 5. Smoke patterns and schematic representation with different yaw angles at $Re = 1020$.

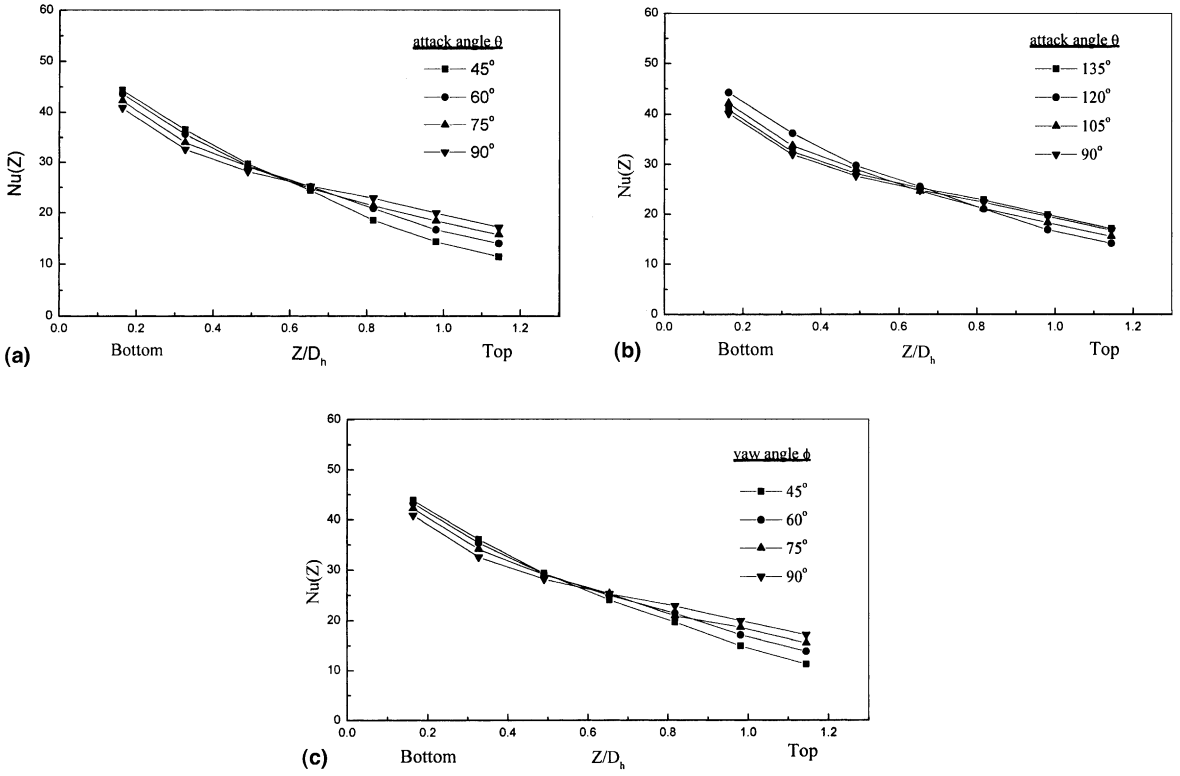

Fig. 6. Rib Nusselt number $Nu(Z)$ for $Re = 3766$ at different axial locations of the rib for (a), (b) $\phi = 90°$ and (c) $\theta = 90°$.

prongs of the horseshoe are longitudinal vortices, which induce transverse velocity components in the flow. The traces of these vortices on the tube should show some increase in heat transfer. The tube heat transfer in the tube wake is low. The strength and hence the beneficial effects of the horseshoe vortex increase with the width of the bluff body (see Fig. 1). However, the size of the wake with poor heat transfer and the pressure loss also increase.

3.2. Heat transfer

3.2.1. Local heat transfer coefficient

The influence of the angle of attack on the local heat transfer performance for $Re = 3766$ is shown in Fig. 6, where $Nu(Z)$ data taken at the location 9.0 mm away from the bottom of the test channel along the axis of the cylinder under different angles are exhibited. Taking an examination, the $Nu(Z)$ are always higher within the restricted region (an angular geometry formed by a horizontal wall subjected to an inclined tube) than on an open surface (near the top). This is because of the present complex flow patterns, which consist of horseshoe vortices in the stagnation area and flow separation in the wake of the tube. Based on data of 45°, 60° and 75° compared to that of the 90° angle of attack, the $Nu(z)$ curve decreases slowly along Z/D_h. The data $Nu(Z)$ of 45° angle in Fig. 6 demonstrate the smallest slope among all the curves, follow by 60°, 75° and 90°, respectively. At a high attack angle ($\theta > 90°$), shown in Fig. 6(b), a similar curve pattern was followed by data taken at a small angle ($\theta < 90°$). Fig. 6(c) shows the cross-average rib Nusselt number $Nu(z)$ for different attack angles along the direction normal to the bottom wall of the test channel. As also expected, large Nusselt numbers are obtained near the bottom of the test tube, while toward the top, the $Nu(Z)$ decreases. Fig. 7 displays variation of the local Nusselt number with Z/D_h for $Re = 3776$ at different attack angles and a fixed yaw angle (45°). This same insensitivity to angle of attack at yaw angle of 45° is also in evidence in Fig. 7.

3.2.2. Correlation of Nusselt number

Figs. 8 and 9 correspond to attack angles of 45°, 60°, 75°, 90°, 105° and 135°. In each figure, the data for the various angles of attack are distinguished by the symbols listed at the upper left. The solid lines appearing in the figures represent least square fits of the data. Fig. 8 shows the effect of Reynolds number on averaged Nusselt number for different attach angles at yaw angle of 90°. Inspection of the Fig. 8 shows that, as expected, the Nusselt number increases with increasing Reynolds

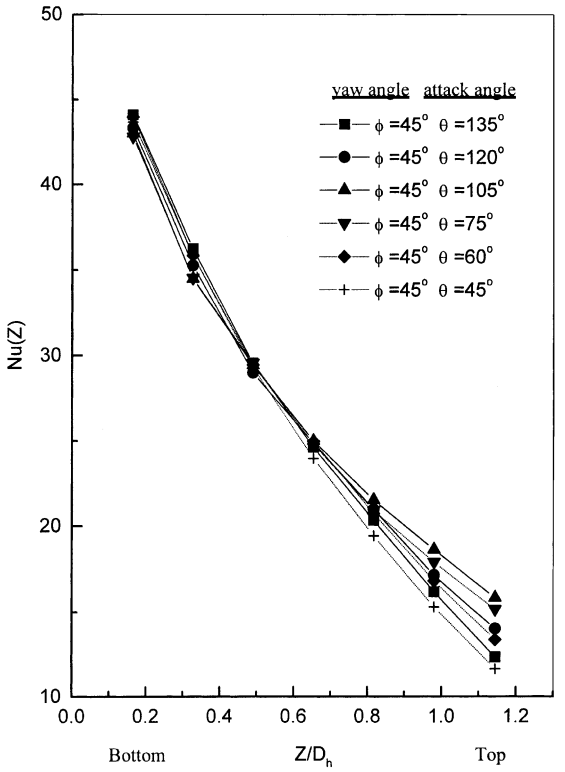

Fig. 7. Variation of the local Nusselt number with Z/D_h for $Re = 3766$ at different attack angles at yaw angle = 45°.

number. Aside from this, all other findings in evidence in the figure have to be regarded with a certain degree of surprise and are, therefore, especially worthy of note. From Fig. 8, it is seen that the Nusselt number is quite insensitive to the angle of attack over the range investigated. Specially, aside from the 1–2% scatter of the data, the Nusselt number varies (i.e., increases) by only 9% and 7% as the angle of attachment varies from 45° to 90° (Fig. 6(a)) and 90° to 135° (Fig. 6(b)), respectively. This variation of the Nusselt number is very much less than would be expected on the basis of the wedge-flow solutions of convectional boundary layer theory (e.g., [12]).

This same insensitivity to angle of attack is also in evidence in Figs. 9(a) and (b); therefore, it applies to all of the yaw angles investigated. Next, consideration may be given to how the value of the Nusselt number responds to changes in the angle of yaw. By making comparisons among Fig. 8(a), (b) and Fig. 9(a), (b) and taking note of the coefficients of the fitted curves, it is seen that the Nusselt number varies by about 2% over the entire range of yaw angle. Thus, for practical purposes, Nusselt number can be taken to be independent of the angle of yaw.

Attention will now be turned to the correlation of the results. Experimental results for the present study (single tube) are interpreted by a functional relation in the exponential form

$$Nu = CRe^m Pr^n, \tag{3}$$

where C and m in a definite region of Re are governed by the tube arrangement (attack and yaw angle) for the present study, and the exponent n denotes the effect of the fluid physical properties on heat transfer. These constants must be evaluated experimentally and analytically from the heat transfer mechanism. As seen in Figs. 8 and 9, the $\overline{Nu(Z)}/Pr^{1/3}$ for the lower angles of attack ($\theta < 90°$) tend to rise together, as do the $\overline{Nu(Z)}/Pr^{1/3}$ for the higher angles of attack ($\theta > 90°$). In Figs. 8 and 9 the solid lines appearing in the figures represent squares fits of the data. Thus, from the data given in the figures and Eq. (3), the effects of the Reynolds number on the average Nusselt number in present study can be correlated by the following equations:

$$\overline{Nu(Z)} = 0.181Re^{0.63}Pr^{1/3} \quad \text{for } 45° \geqslant \theta \leqslant 90°, \ \phi = 90°, \tag{4}$$

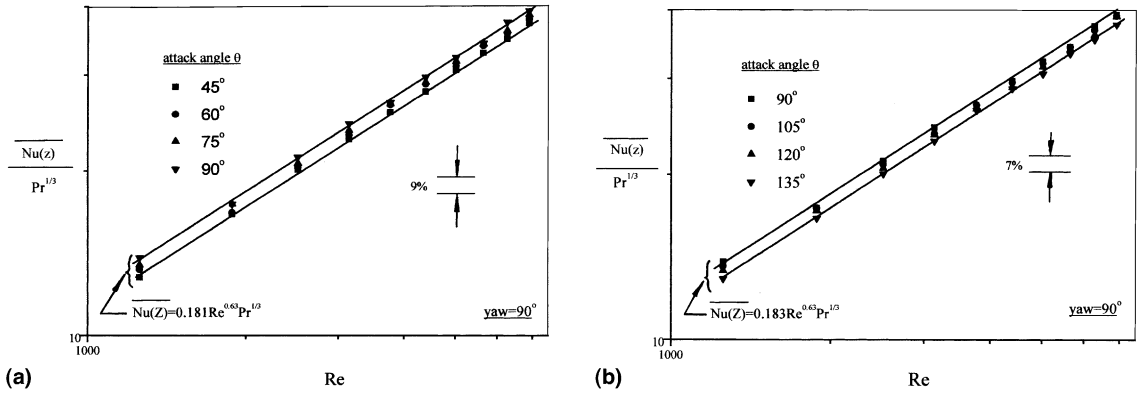

Fig. 8. Effect of Reynolds number on averaged Nusselt number for different attack angles at yaw angle = 90°.

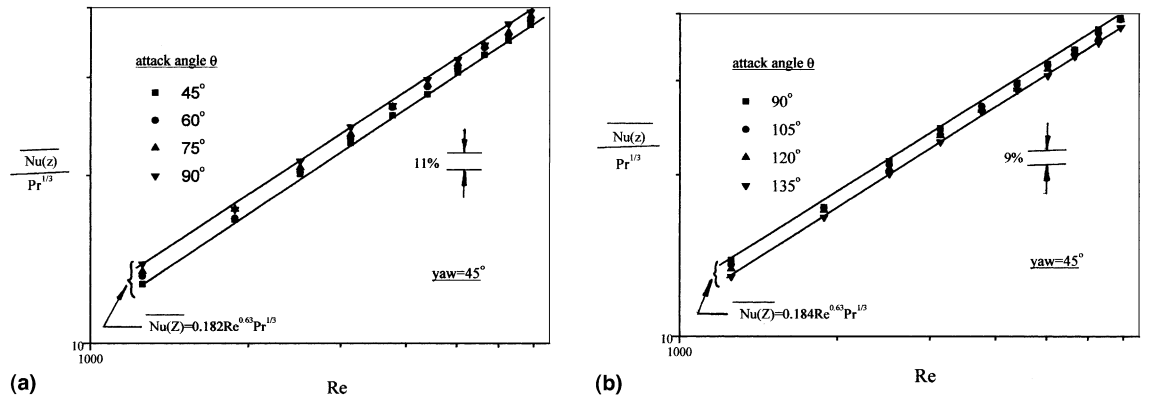

Fig. 9. Effect of Reynolds number on averaged Nusselt number for different attack angles at yaw angle = 45°.

$$\overline{Nu(Z)} = 0.183Re^{0.63}Pr^{1/3} \quad \text{for } 90° \geqslant \theta \leqslant 135°,\ \phi = 90°, \tag{5}$$

$$\overline{Nu(Z)} = 0.182Re^{0.63}Pr^{1/3} \quad \text{for } 45° \geqslant \theta \leqslant 90°,\ \phi = 45°, \tag{6}$$

$$\overline{Nu(Z)} = 0.184Re^{0.63}Pr^{1/3} \quad \text{for } 90° \geqslant \theta \leqslant 135°,\ \phi = 45°. \tag{7}$$

The resulting equation is shown in each figure. The variation of C is about 2%. The maximum deviations of the experimental data from Eqs. (4)–(7) for yaw angle of 90° and 45° are 6.7%, 4.5%, 5.6%, and 4.7%, respectively. In view of the insensitivity of the results to the angles of attack and yaw, a simple formula can be given which represents all the data to an accuracy of ±4%. The formula is

$$\overline{Nu(Z)} = 0.182Re^{0.63}Pr^{1/3}. \tag{8}$$

The simplicity and generality of this equation makes it a useful tool for design. The standard correlation [13] ($Nu = CRe^{m}Pr^{1/3}$) for a cylinder in cross-flow ($\phi = 90°$, $\theta = 90°$) is widely used, where the constants $C = 0.683$, $m = 0.466$ for $Re = 40$–4000 and $C = 0.193$, $m = 0.618$ for $Re = 4000$–$40\,000$. In general, the $Nu(Z)$ values of the correlation for present study (Eqs. (4)–(8)) are a little lower than the results of [13]. This difference seems due to the inclination/yaw angles considered. Taking the present case ($\phi = 90°$, $\theta = 90°$) into account it was found that the heat transfer coefficient between the present study and previous result [13] for a cylinder in cross-flow is slightly different, but, within the error bounds (about ±5%), seems consistent.

3.2.3. Correction factor C_θ for calculating the Nusselt number

Heat transfer of an inclined tube may be predicated, as in the case of cross-flow, from Eq. (1) with an auxiliary factor from Fig. 10 for the attack angle. Factor C_θ is a ratio of the heat transfer from a tube at arbitrary θ to that from a tube at $\theta = 90°$:

$$C_\theta = \frac{\overline{Nu(Z)}}{\overline{Nu(Z)}_{\theta=90°}}. \tag{9}$$

The relationship of factor C_θ and the attack angle θ under a wide range of yaw angles ($\phi = 45$–$90°$) gives a shaded area between two curves for the present study shown in Fig. 10. An average value of C_θ was obtained over the range of the yaw angles ($\phi = 45$–$90°$) under

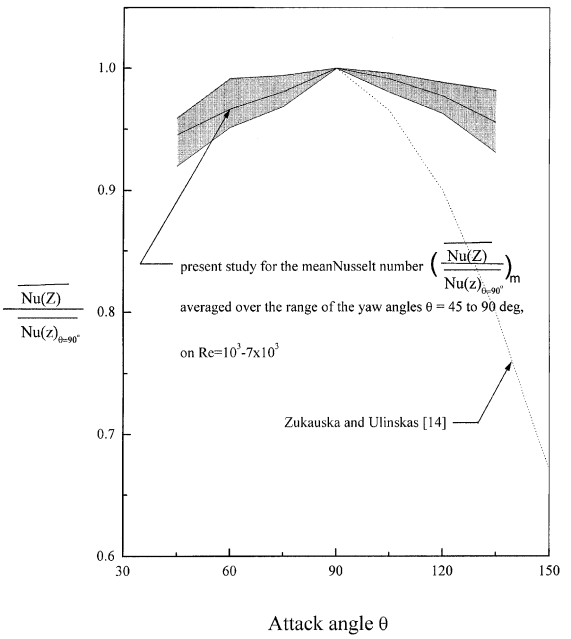

Fig. 10. Effect of attack angle on average Nusselt number ratios for yaw angle = 45–90°.

Table 1
Average Nusselt number ratio ($(\overline{Nu(Z)}/\overline{Nu(Z)}_{\theta=90^\circ})_m$) and max/min Nusselt number ratios ($(\overline{Nu(Z)}/\overline{Nu(Z)}_{\theta=90^\circ})_{max}/(\overline{Nu(Z)}/\overline{Nu(Z)}_{\theta=90^\circ})_{min}$) of the different attack angles for $\phi = 45$–90°

Attack angle, θ	Yaw angle, ϕ	$\left(\frac{\overline{Nu(Z)}}{\overline{Nu(Z)}_{\theta=90^\circ}}\right)_m^a$	$\left(\frac{\overline{Nu(Z)}}{\overline{Nu(Z)}_{\theta=90^\circ}}\right)_{max}$	$\left(\frac{\overline{Nu(Z)}}{\overline{Nu(Z)}_{\theta=90^\circ}}\right)_{min}$
45°	45–90°	0.946	0.959	0.920
60°	45–90°	0.967	0.991	0.952
75°	45–90°	0.981	0.994	0.969
90°	45–90°	1	1	1
105°	45–90°	0.991	0.996	0.980
120°	45–90°	0.977	0.988	0.963
135°	45–90°	0.956	0.982	0.931

[a] Mean value averaged over the range of yaw angle $\phi = 45$–90°, at a fixed attack angle θ.

study. It can be used for finding the heat transfer on a tube positioned at different angles to the flow direction. No significant effect of the *Re* on the factor C_θ has been found. Fig. 10 depicts the comparison of the factor C_θ for present investigation with that of Zukauskas and Ulinskas [14] for the heat transfer coefficient of staggered and in-line banks. Unfortunately, because of the different geometries used, it is difficult to assess completely the significance of the results. However, it appears that the factor C_θ decreases as the attack angle ($\theta > 90^\circ$) increases. In addition, in order to express more pronouncedly, the numerical data for average Nusselt number ratio ($(\overline{Nu(Z)}/\overline{Nu(Z)}_{\theta=90^\circ})_m$) and max/min Nusselt number ratios ($(\overline{Nu(Z)}/\overline{Nu(Z)}_{\theta=90^\circ})_{max}/(\overline{Nu(Z)}/\overline{Nu(Z)}_{\theta=90^\circ})_{min}$) of the different attack angles for $\phi =$ 45–90° are also displayed in Table 1.

4. Conclusions

An experimental heat transfer study is done for forced convection airflow over a cylindrical obstacle that is inclined and yawed relative to the oncoming flow. The Reynolds number spanned the range between about 1000 and 7000. For the angle of attack, values of 45°, 60°, 75°, 90°, 105°, 120° and 135° were chosen. With regard to yaw, the symmetry of the geometry requires that only angles 45°, 60°, 75°, and 90° be considered. The coupled contributing factors for heat transfer are separated. Flow visualizations provide a better understanding of the heat transfer mechanism in this study. The main findings based on the experiment are:

1. The stagnation point is the forward-most point on the surface of the cylinder at 90° angle of attack and moves forward as the angle of attack decreases. The position of the stagnation point also responds to variation of the angle of yaw. One can reduce the wake size by using, instead of round tubes, elliptical tubes (or flat tubes) with their major axes parallel to the main flow direction. The heat transfer deterioration in the wake will be smaller for an elliptical tube of the same cross-section as for a round tube. The heat transfer enhancement due to the horseshoe vortex in the stagnation area will also be smaller. However, the real gain will appear in the smaller pressure loss due to the smaller wake for the flat tube than for the round tube.

2. Because of the present complex flow patterns which consist of horseshoe vortices in the stagnation area and flow separation in the wake of the tube, the local $Nu(Z)$ data are always higher within the restricted region (near the bottom) than on an open surface (near the top).

3. The $\overline{Nu(Z)}$ results were insensitive to these angles. This enabled all the results of present study to be represented by the remarkably simple formula $\overline{Nu(Z)} = 0.182Re^{0.63}Pr^{1/3}$, with an accuracy of ±4%.

4. This investigation introduces a factor ($C_\theta = \overline{Nu(Z)}/\overline{Nu(Z)}_{\theta=90^\circ}$) for the angle between the tube and the flow. This means that data for the tube in the present channel, together with C_θ obtained from Fig. 10, can be used for finding the heat transfer on a tube positioned at different angles to the flow direction. In addition, no perceptible dependence of C_θ on *Re* was detected.

Acknowledgements

This research was sponsored by the Cheng-Shiu Institute of Technology of Taiwan under contract no. CSIT-89-19

References

[1] R.L. Webb, E.R.G. Eckert, R.J. Goldstein, Heat transfer and friction in tubes with repeated-ribs roughness, Int. J. Heat Mass Transfer 14 (1971) 601–617.
[2] D.Q. Kern, A.D. Kraus, Extended Surface Heat Transfer, McGraw-Hill, New York, 1972.
[3] A.D. Kraus, Appl. Mech. Rev. 41 (1988) 321.

[4] P.L. Dhar, C.P. Arora, J. Franklin Inst. 301 (1976) 379.
[5] S.J. Kline, F.A. McClintock, Describing uncertainties in single-sample experiments, Mech. Eng. 75 (1953) 3–8.
[6] D.L. Gee, R.L. Webb, Forced convection heat transfer in helically rib-roughened tubes, Trans. ASME J. Heat Transfer 23 (1980) 1127–1136.
[7] J.C. Han, J.S. Park, Developing heat transfer in rectangular channels with rib turbulators, Int. J. Heat Mass Transfer 31 (1988) 183–195.
[8] T. Ota, S. Aiba, T. Tsuruta, M. Kaga, Forced convection heat transfer from an elliptic cylinder of axis ratio 1:2, Bull. Jpn. Soc. Mech. Eng. 26 (1983) 262–267.
[9] H.M. Badr, Mixed convection from a straight isothermal tube of elliptic cross section, Int. J. Heat Transfer 37 (1994) 2343–2365.
[10] J. Merkin, Free convection boundary layers on cylinders of elliptic cross section, Trans. ASME J. Heat Transfer 99 (1977) 453–457.
[11] A. Bar-Cohen, M. Jelinek, Heat Transfer Eng. 6 (1985) 68.
[12] E.R.G. Eckert, R.M. Drake, in: Analysis of Heat and Mass Transfer, McGraw-Hill, New York, 1972, p. 310.
[13] F.P. Incropera, D.P. DeWitt, in: Introduction to Heat and Mass Transfer, 4th ed., Wiley, New York, 1996, p. 370.
[14] A. Zukauskas, R. Ulinskas, Efficiency parameters for heat transfer in tube banks, Trans. ASME J. Heat Transfer 6 (1985) 19–25.